Azimuth Enhancement for Automotive SAR Imaging

Shahzad Gishkori and Bernard Mulgrew
Institute for Digital Communications, The University of Edinburgh, UK.
Emails: {s.gishkori, bernie.mulgrew}@ed.ac.uk

***Abstract*—In this paper, we present signal processing methods for automotive radar imaging. Our focus is to enhance angular resolution of the radar image. We consider frequency modulated continuous wave signalling. We propose a forward scanning synthetic aperture radar methodology, which combines scene scanning and synthetic aperture processing. To take full advantage of this methodology, we propose two algorithms: i) a modified back projection algorithm, which capitalises on the target information available in range domain as well as in the azimuth domain, and ii) an algorithm based on state-of-the-art technique of compressed sensing, which preserves features of the target objects as well as parsimony of the target scene. Simulation results verify our proposed methodology.**

***Index Terms*—Automotive SAR, angular resolution, back projection, compressed sensing.**

I. Introduction

Automotive (Auto-) radar has received a lot of attention recently, especially in the context of autonomous cars [1], [2]. Mainly, its role has been restricted to detection and/or collision avoidance only. Scene imaging has mostly been performed by lidar and camera, whose imaging capabilities are reduced in severe weather conditions, e.g., in fog, rain, etc. The radar can perform even in such harsh conditions and create an image of the target scene. Recently, automotive-terrain imaging capabilities of a low-THz radar were presented in [3] by using frequency modulated continuous wave (FMCW) signalling. Low-THz frequencies provide the radar with enhanced penetration capabilities and the radar can cope with severe weather conditions.

A main challenge for the Auto-radar is its range and angular resolution. Range resolution can be increased by increasing transmit signal bandwidth. However, azimuth resolution (AR) depends on physical aperture of the radar. One way out is to use a synthetic aperture radar (SAR). Given the movement of the vehicle, SAR processing can easily be implemented in the Auto-radar. Generally, a side looking (SL) SAR achieves maximum gains of the synthetic aperture. However, an Auto-radar mostly works as a forward looking (FL) radar. This reduces the effective synthetic aperture. Thus, AR enhancement of an Auto-radar with SAR mechanism has very limited gains. This paper tackles the issue of AR enhancement in this scenario.

This work was supported by Jaguar Land Rover and the UK-EPSRC grant EP/N012240/1 as part of the jointly funded Towards Autonomy: Smart and Connected Control (TASCC) Programme.

AR enhance of FL-SAR has been a subject of research for the past many years. In [4], a sector imaging radar for enhanced vision (SIREV) has been presented, where synthetic aperture is created by sequentially selecting the receive antenna elements. However, AR is still limited by the length of the antenna array. Some direction of arrival (DOA) based approaches, e.g., [5], [6] can also be used. However, their performance can be limited by the number of frequency channels. Substantial literature consists of deconvolution approaches to improve the AR, e.g., [7], [8], [9]. Since the received signal can be considered as a convolution between the antenna pattern and the target scene, a deconvolution process can potentially improve the AR. However, AR improvement through deconvolution is an under-determined problem, i.e., the number of unknowns are more than the number of available measurements. This can be circumvented by using different regularization techniques. A common regularization technique is to use an ℓ_2-norm penalty. This can result in a unique solution to the problem. However, automotive target scenes are sparse in nature and an ℓ_2-norm penalty cannot preserve sparsity in the under-determined setting. Nonetheless, using an ℓ_1-norm penalty can offer a sparse solution. This is a well known fact in the theory of compressed sensing (CS) [10]. CS has been used in a number of radar related problems, e.g., [11], [12]. In [13], CS was used to improve the AR of a scanning phased array radar. In this paper, we use a similar approach to increase AR of an Auto-radar for a given range bin. However, our method includes SAR processing as well, which can further enhance AR and result in improved imaging.

In terms of SAR processing, a number of algorithms are available, e.g., Doppler beam sharpening, range migration algorithm, back projection (BP), etc. Most of these techniques can be applied only under certain conditions. However, BP algorithm is quite flexible and it can be applied to a variety of imaging scenarios. Therefore, we work with BP for the purpose of automotive scene imaging. A limiting factor for BP is its computational complexity. However, a number of fast implementations of BP are available.

In this paper, we provide techniques to enhance AR of the Auto-radar while forming a 2-D radar image. We use a monostatic FMCW radar that operates at low-THz frequencies. The radar scans the target scene at multiple look angles (LAs) and then moves to the next scanning position over the aperture. We call this process as forward scanning SAR (FS-SAR).

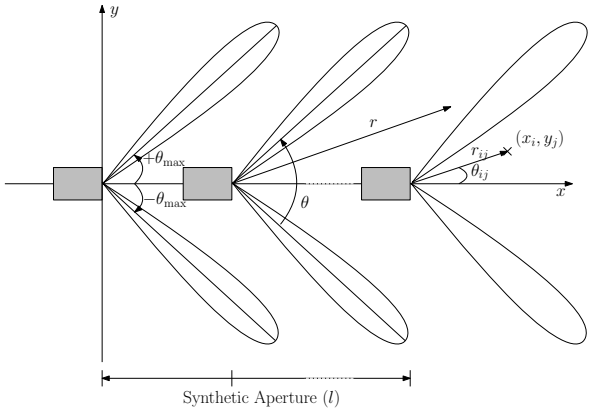

Fig. 1. FS-SAR schematic (2-D).

Note, we assume a mechanically steered beam. However, electronic scanning can also be implemented. We enhance the AR by using the CS techniques for each scan. Then, SAR processing is done over the reconstructed scans of the complete aperture. We also provide a modified back projection algorithm which utillizes the returns from all LAs as well as all aperture positions. The modified back projection does not require any pre-processing.

Organisation. Section II presents the system model, Section III describes the proposed algorithms, i.e, modified back projection and compressed sensing based back projection, Section IV provides simulations and conclusions are given in Section V.

Notations. Matrices are in upper case bold while column vectors are in lower case bold, $[\mathbf{X}]_{i,j}$ is the ijth entry of the matrix $\mathbf{X}$, $\mathbf{I}_N$ is the identity matrix of size $N \times N$, $\mathbf{0}_N$ is a vector of size $N \times 1$, $(\cdot)^T$ denotes Transpose, $(\cdot)^H$ is Hermitian, $(\cdot)^{-1}$ denotes inverse, $\otimes$ stands for the Kronecker product, $\star$ describes the convolution, $\hat{\mathbf{x}}$ is the estimate of $\mathbf{x}$, $\triangleq$ defines an entity, $\mathcal{F}\{\cdot\}$ describes a Fourier transform operation, $\uparrow_{\kappa,\kappa'}(\mathbf{X})$ upsamples the matrix $\mathbf{X}$ by an order κ along its rows and by an order κ' along its columns and the ℓ_p-norm of a vector $\mathbf{x}$ is denoted as $||\mathbf{x}||_p = (\sum_{i=0}^{N-1} |[\mathbf{x}]_i|^p)^{1/p}$.

II. System Model

Figure 1 represents the schematic of the proposed FS-SAR for 2-D processing, where $l \in [-L/2, L/2]$ is the aperture sample, $\theta \in [-\theta_{\max}, +\theta_{\max}]$ is the LA, $r \in (0, R_{\max}]$ is the Euclidean distance between the target and the radar, (x_i, y_j) is the target location in a Cartesian coordinate system (CCS) which can also be represented in a polar coordinate system (PCS) with range $r_{ij} \triangleq \sqrt{x_i^2 + y_j^2}$ and angle $\theta_{ij} \triangleq \tan^{-1}(y_j/x_i)$.

Let the generic FMCW transmit pulse be

$$s^{\mathrm{Tx}}(t) = \exp\left(j2\pi f_0 t + j\pi\beta t^2\right) \tag{1}$$

where f_0 is the carrier frequency, $\beta \triangleq B/T$ is the chirp rate, B is the bandwidth of the transmitted signal, T is the pulse repetition interval (PRI) and $t \in (0, T]$ is the fast time variable. The received signal at lth scan step and θth LA can be written as

$$s_{l,\theta}^{\mathrm{Rx}}(t) = \sum_{u=1}^{U} \alpha_u \exp\left(j2\pi f_0[t - \tau_{l,\theta}(u)] + j\pi\beta[t - \tau_{l,\theta}(u)]^2\right) \tag{2}$$

where α_u is the reflectivity coefficient and $\tau_{l,\theta}(u)$ is the two-way time delay of the uth scatterer. After deramping, low-pass filtering and deskewing, the resulting signal in (2) can be written as

$$s_{l,\theta}(t) = \sum_{u=1}^{U} \alpha_u \exp(j2\pi f_0 \tau_{l,\theta}(u)) \exp(j2\pi\beta\tau_{l,\theta}(u)t) \tag{3}$$

where the exponent $j2\pi\beta\tau_{l,\theta}(u)t$ carries information regarding target range and the exponent $j2\pi f_0\tau_{l,\theta}(u)$ is important for SAR processing. Now, the range profile can be generated by taking the Fourier transform of $s_{l,\theta}(t)$ and then using a linear transform to the range domain, i.e.,

$$x_{l,\theta}(r) = \mathcal{F}\{s_{l,\theta}(t)\}|_{r=\frac{fc}{2\beta}}. \tag{4}$$

Let $\Delta_r \triangleq c/2B$ be the range resolution and r_{n_r}, for $n_r = 0, 1, \cdots, N_r - 1$, reference the range bins, where, $N_r \triangleq R_{\max}/\Delta_r$. From (4), we can represent the target scene reflectivities along azimuth for the r_{n_r}th range bin by $x_{l,r_{n_r}}(\theta)$, i.e.,

$$x_{l,r_{n_r}}(\theta) = \{x_{l,\theta}(r_{n_r})\}_{\theta=-\theta_{\max}}^{+\theta_{\max}}. \tag{5}$$

Note, we drop the subscript n_r from $x_{l,r_{n_r}}(\theta)$ in the following. If $h(\theta)$ represents the antenna beam of angular length 2ϕ then the signal measured along the azimuth can be written as

$$y_{l,r}(\theta) = h(\theta) \star x_{l,r}(\theta) + n_{l,r}(\theta) \tag{6}$$

where $y_{l,r}(\theta)$ is the measured signal and $n_{l,r}(\theta)$ is additive white Gaussian noise. We can represent $h(\theta)$ as an $N_h \times 1$ vector $\mathbf{h}$ with $N_h = \lfloor 2\phi/\delta_\theta \rfloor + 1$, $y_{l,r}(\theta)$ as an $N_\theta \times 1$ vector $\mathbf{y}_{l,r}$ with $N_\theta = \lfloor 2\theta_{\max}/\Delta_\theta \rfloor + 1$ and $x_{l,r}(\theta)$ as an $N_x \times 1$ vector, $\mathbf{x}_{l,r}$, with $N_x = \xi N_\theta + N_h - 1$. Note, Δ_θ is the angular sampling interval of the measurements and δ_θ is the desired sampling interval required for AR, where $\xi = \Delta_\theta/\delta_\theta$ and $\xi \gg 1$. Thus, we can write (6) in the following sampled form.

$$\mathbf{y}_{l,r} = \mathbf{G}\mathbf{H}\mathbf{x}_{l,r} + \mathbf{n}_{l,r} \tag{7}$$

where $\mathbf{n}_{l,r}$ is an $N_\theta \times 1$ noise vector and $\mathbf{H}$ is the $(\xi N_\theta - 1) \times N_x$ convolution matrix, defined as

$$\mathbf{H} \triangleq \begin{pmatrix} \mathbf{h}^H & & \mathbf{0}^T_{(N_x - N_h)} \\ 0 & \mathbf{h}^H & \mathbf{0}^T_{(N_x - N_h - 1)} \\ \vdots & \vdots & \vdots \\ \mathbf{0}^T_{(N_x - N_h)} & & \mathbf{h}^H \end{pmatrix} \tag{8}$$

and $\mathbf{G}$ is an $N_\theta \times (\xi N_\theta - 1)$ selection matrix. Now, for all range bins, we can modify (7) as

$$\mathbf{Y}_l = \mathbf{G}\mathbf{H}\mathbf{X}_l + \mathbf{N}_l \tag{9}$$

where $\mathbf{Y}_l$, $\mathbf{X}_l$ and $\mathbf{N}_l$ are $N_\theta \times N_r$, $N_x \times N_r$ and $N_\theta \times N_r$ matrices, respectively.

III. FS-SAR Algorithms

Traditionally, a SAR operates in two basic mode, i.e., stripmap mode and spotlight mode. Our proposed FS-SAR is partly related to both of these modes but is not the same. We scan the target scene at different LAs and then move over the aperture to the next scan step. However, neither the target area remains fixed as in spotlight mode, nor the LA remains fixed as in stripmap mode. In this section, we provide two algorithms regarding the FS-SAR methodology. Our approach is based on BP. The flexibility of BP for different SAR mode of operations makes it a feasible candidate for imaging automotive target scenes.

A. Modified Back Projection

We first introduce a modified version of BP. In principle, all of the measurements from each scanning step on the aperture are projected back to the target location. Thus, a coherent combination of all measurements corresponding to the target location generates a combined response of the synthetic aperture. To this end, the measurements are first upsampled via interpolation and subsequently integrated over the aperture to generate a SAR image. In our case, we gain information both from the range and the angular domain. Therefore, the interpolation can be done over both the domains. This phenomenon leads to the modification of the standard BP.
Let $\uparrow_{\kappa,\kappa}(\mathbf{Y}_l)$ represent the upsampled form of $\mathbf{Y}_l$ in (9), where κ is the order of interpolation along rows and columns. Then, the reconstructed image of the target scene in CCS, via modified BP (MBP), can be written as

$$\gamma_{ij}^{\mathrm{MBP}} = \sum_{\theta} \sum_{l} [\uparrow_{\kappa,\kappa} (\mathbf{Y}_l)]_{\theta, I_{r_{ij}}} \tag{10}$$

where $I_{r_{ij}}$ is the column index corresponding to range $r_{ij} = \sqrt{(x_i - l)^2 + y_j^2}$. Thus, in MBP, the measurements are upsampled via interpolation over both the azimuth and the range domains as a first step and then integration is carried out over both the aperture and angle for each target location. This accumulation of back scattered energy results in enhanced AR and better radar image reconstruction.

B. Compressed Sensing Based Back Projection

The FS-SAR method increases target response by generating target information over both the aperture and the angular domains. The MBP algorithm has the ability of capturing all of the target back-scattered energy. However, it cannot create a big contrast of reflectivity between neighbouring scatterers. This goal can be achieved by using CS, which produces a radar image consisting of few bright scatterers only. Our approach is to use CS for reconstructing individual scans and then using BP for SAR processing.
Let (9) is written in the following vectorised form.

$$\mathbf{y}_l = \underbrace{[\mathbf{I}_{N_r} \otimes (\mathbf{G}\mathbf{H})]}_{\triangleq \mathbf{\Phi}} \mathbf{x}_l + \mathbf{n}_l \tag{11}$$

where $\mathbf{y}_l \triangleq \mathrm{vec}(\mathbf{Y}_l)$, $\mathbf{x}_l \triangleq \mathrm{vec}(\mathbf{X}_l)$ and $\mathbf{n}_l \triangleq \mathrm{vec}(\mathbf{N}_l)$ are $N_\theta N_r \times 1$, $N_x N_r \times 1$ and $N_\theta N_r \times 1$ vectors, respectively., and $\mathbf{\Phi}$ is an $N_\theta N_r \times N_x N_r$ measurement matrix. Since $N_\theta \ll N_x$, (11) is an under-determined system of linear equations. Under the CS framework, an estimate of $\mathbf{x}_l$ can be obtained by solving the following optimisation problem (OP).

$$\hat{\mathbf{x}}_l = \arg\min_{\mathbf{x}_l} \|\mathbf{y}_l - \mathbf{\Phi}\mathbf{x}_l\|_2^2 + \lambda \|\mathbf{x}_l\|_1^1 \tag{12}$$

where $\lambda > 0$. Generally, the CS framework puts certain conditions on the measurement matrix to guarantee a unique and sparse solution. One parameter of these conditions is known as mutual coherence, which basically indicates the interdependence of the columns of measurement matrix. The lower the mutual coherence, the better the results. Another parameter is known as restricted isometry property, which basically indicates if every submatrix of the measurement matrix with less than $K = \|\mathbf{x}_l\|_0^0$ columns acts like an orthonormal matrix. In essence, these parameters give a bound on the number of measurements required to estimate the number of unknown nonzero elements, i.e., K, for different measurement matrices, e.g., Gaussian, Bernoulli and partial Fourier matrices [14]. In the context of our application, some works, e.g., [13], provide heuristic assessments of using a uniform sampling matrix as a measurement matrix to obtain reasonable performance results. In this paper, we continue with such an approach and we obtain measurements at uniform angular intervals.
The OP in (12) is known as least absolute shrinkage and selection operator (LASSO). It basically generates element-wise sparse estimate of $\mathbf{x}_l$, depending on the λ. However, it does not exploit any specific structure in the elements of $\mathbf{x}_l$. In our application, a target scene consists of objects which have a continuum of a reflective surface. Therefore, we need an OP which exploits the correlations between consecutive elements of $\mathbf{x}_l$. In this paper, we propose to use fused LASSO (F-LASSO) [15] for Auto-radar imaging. It can be written as

$$\hat{\mathbf{x}}_l = \arg\min_{\mathbf{x}_l} \|\mathbf{y}_l - \mathbf{\Phi}\mathbf{x}_l\|_2^2 + \lambda \|\mathbf{x}_l\|_1^1 + \lambda_f \|\mathbf{D}\mathbf{x}_l\|_1^1 \tag{13}$$

where $\lambda_f > 0$ is a fusion penalty parameter and $\mathbf{D}$ is the $N_x N_r \times N_x N_r$ fusion matrix, i.e.,

$$\|\mathbf{D}\mathbf{x}_l\|_1^1 = \sum_{m=1}^{N_x N_r - 1} \|[\mathbf{x}_l]_m - [\mathbf{x}_l]_{m-1}\|_1^1. \tag{14}$$

We can see (14) concerns the difference of consecutive elements in $\mathbf{x}_l$. Thus, both the individual elements as well as the difference of elements of $\mathbf{x}_l$ are penalised by F-LASSO. Therefore, we obtain enhanced AR as well as an improved radar image. We suggest solving (13) by using alternating direction method of multipliers (ADMM) [16] based methods. Now, the estimate $\hat{\mathbf{x}}_l$ can be reshaped into an $N_x \times N_r$ matrix $\hat{\mathbf{X}}_l$. By using $\hat{\mathbf{X}}_l$, the radar image can be reconstructed via CS based BP (CBP) as

$$\gamma_{ij}^{\mathrm{CBP}} = \sum_{l} [\uparrow_{1,\kappa} (\hat{\mathbf{X}}_l)]_{I_{\theta_{ij}}, I_{r_{ij}}} \tag{15}$$

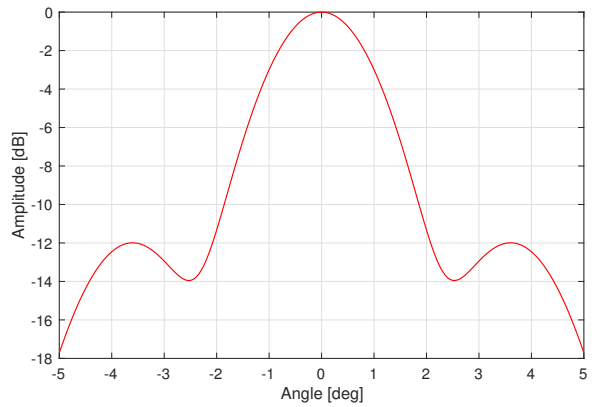

Fig. 2. Antenna Pattern.

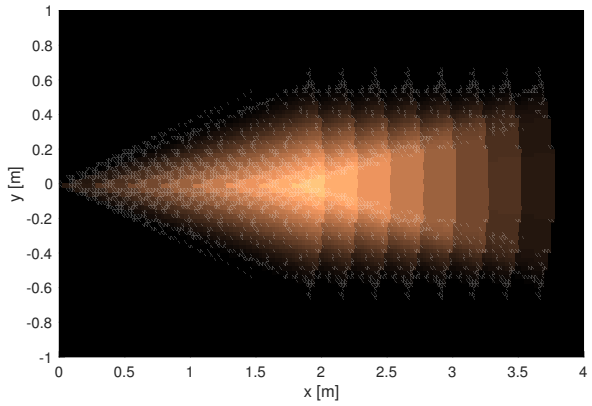

Fig. 3. Auto-radar measurement path.

where $I_{\theta_{ij}}$ is the row index and $I_{r_{ij}}$ is the column index in $\uparrow_{1,\kappa}(\hat{\mathbf{X}}_l)$, corresponding to angle $\theta_{ij} = \tan^{-1}((x_i - l)/y_j)$ and range r_{ij}, respectively. Thus, in CBP, measurements are upsampled in the range domain only, whereas upsampling in the azimuth domain is unnecessary due to CS based pre-processing. Further, integration is done over the aperture domain as a second step. A combination of CS based reconstruction over the angle domain with SAR processing provides improved AR and Auto-radar imaging.

IV. Simulations

We consider an FMCW monostatic radar with carrier frequency $f_0 = 150$ GHz and 3 dB beamwidth $\theta_{3\text{dB}} = 2^\circ$. As the knowledge of beam pattern is essential for AR improvement, we consider the beam pattern described by [17]. Figure 2 shows such a beam pattern, used in our simulations.

Since the radar signal bandwidth $B = 6$ GHz, in our case, the range resolution $\Delta_r = 2.5$ cm. We create the target scene as a grid consisting of cells, in the CCS, where the size of these cells equals the range resolution in both axes. A target object may spread over a number of cells.

For the simulation, our target scene occupies an area of 2×4 m^2. Note, this size is for the sake of demonstration only. However, our methods are applicable for larger sizes as well. Radar motion is confined to the x-axis at $y = 0$. Note, this movement pattern does not limit the proposed methods and is presented as an example only. Figure 3 shows the radar path. We consider radar angular scan range from -15° to $+15^\circ$, with angular steps, $\Delta_\theta = 0.5^\circ$. Maximum range for each scan $R_{\max} = 2$ m. We consider $N_l = 8$ aperture steps with aperture sampling interval $\Delta_l = 25$ cm. In the proposed FS-SAR methodology, the target area with higher visits from the radar acquires higher back scattered energy. This can be seen in Figure 3 by areas illuminated with higher intensity.

Our target scene, in Figure 4, shows the requirements of a typical road scene. There are eight target objects. Each target is spread over 5×3 group of cells. The distance between the objects along x-axis is of two cells, i.e, 5 cm and the distance between the objects along y-axis consists of one cell, i.e., 2.5 cm. Note, this amounts to requiring a better AR of almost half an order of magnitude at a range of 4 m. We generate the measurements according to (6). We assume an SNR of 10 dB defined in terms of (11) as

$$\text{SNR} \triangleq \frac{\|\mathbf{\Phi}\mathbf{x}_l\|_2^2}{N_\theta N_r \sigma^2}. \tag{16}$$

The measurements are generated for every LA at every aperture step. A superimposed representation of all the measurements is given in Figure 5. We can see that the objects are distinct in the range domain because of the fine range resolution. However, the objects cannot be resolved in the azimuth.

Figure 6 shows the result of image reconstruction via MBP. In comparison to the raw measurements, the image constructed via MBP is much better. The contrast between target objects in the azimuth is not stark. However, a dark border between the objects is clearly visible. Figure 7 shows the result of image reconstruction via CBP. We see improved results in comparison to MBP. Each object has been reconstructed completely. Target objects are clearly distinguishable both in the range and the azimuth. The specular artefacts of the target scene have also been supressed. Thus, F-LASSO not only creates parsimony in the solution but also preserves the target features. Note the tuning parameters λ and λ_f in (13) can be selected via cross validation.

V. Conclusions

In this paper, we have presented signal processing techniques to improve azimuth resolution for Auto-radar imaging. We have used FMCW signalling for a THz radar. We have proposed an FS-SAR methodology which generates maximum back-scattered energy of the radar illuminated targets. We have proposed two algorithms, namely, modified back projection and compressed sensing based back projection, in order to benefit from the FS-SAR methodology. Our algorithms are applicable in a variety of road scenes. Simulation results prove the validity of our proposed methods.

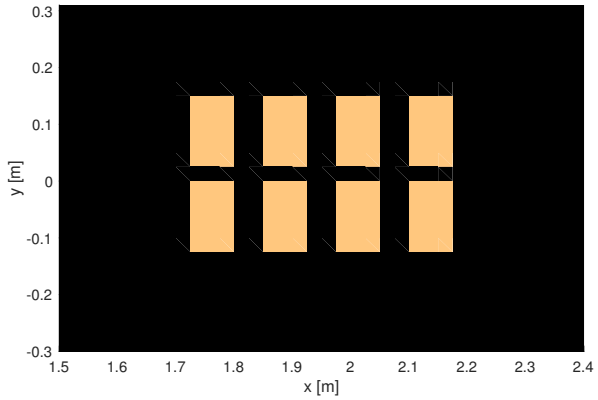

Fig. 4. Target Scene in the CCS.

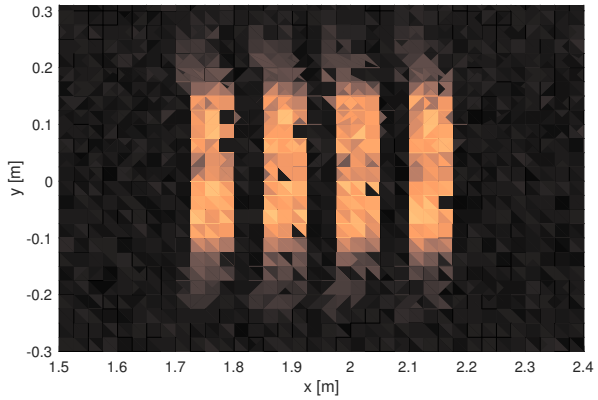

Fig. 5. Measured Scene.

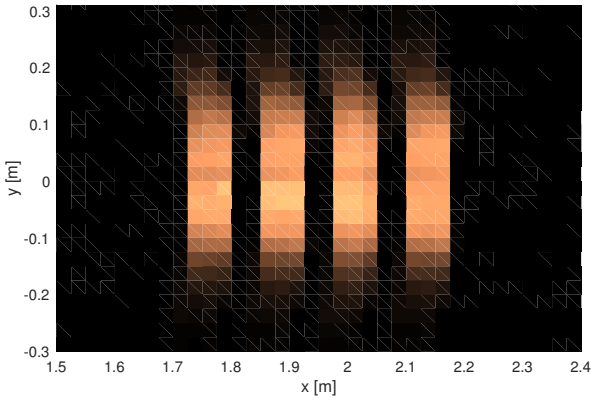

Fig. 6. Reconstructed image via MBP.

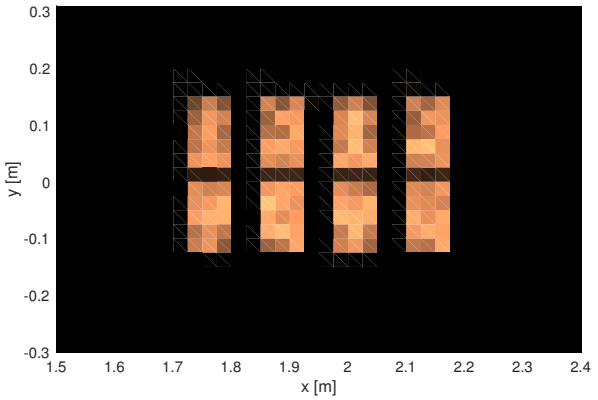

Fig. 7. Reconstructed image via CBP.

ACKNOWLEDGEMENTS

This work has been approved for submission by TASSC-PATHCAD sponsor, Chris Holmes, Senior Manager Research, Research Department, Jaguar Land Rover, Coventry, UK.

REFERENCES

[1] K. Bengler, K. Dietmayer, B. Farber, M. Maurer, C. Stiller, and H. Winner, "Three decades of driver assistance systems: Review and future perspectives," *IEEE Intelligent Transportation Systems Magazine*, vol. 6, no. 4, pp. 6–22, winter 2014.

[2] E. Guizzo, "How Google's self-driving car works," *IEEE Spectrum Online*, vol. 18, 2011.

[3] D. Jasteh, E. G. Hoare, M. Cherniakov, and M. Gashinova, "Experimental low-terahertz radar image analysis for automotive terrain sensing," *IEEE Geoscience and Remote Sensing Letters*, vol. 13, no. 4, pp. 490–494, April 2016.

[4] G. Krieger, J. Mittermayer, S. Buckreuss, M. Wendler, T. Sutor, F. Witte, and A. Moreira, "Sector imaging radar for enhanced vision," *Aerospace Science and Technology*, vol. 7, no. 2, pp. 147 – 158, 2003.

[5] A. Farina, F. Gini, and M. Greco, "DOA estimation by exploiting the amplitude modulation induced by antenna scanning," *IEEE Transactions on Aerospace and Electronic Systems*, vol. 38, no. 4, pp. 1276–1286, Oct 2002.

[6] S. Uttam and N. A. Goodman, "Superresolution of coherent sources in real-beam data," *IEEE Transactions on Aerospace and Electronic Systems*, vol. 46, no. 3, pp. 1557–1566, July 2010.

[7] M. A. Richards, "Iterative noncoherent angular superresolution [radar]," in *Radar Conference, 1988., Proceedings of the 1988 IEEE National*, Apr 1988, pp. 100–105.

[8] M. Ruggiano, E. Stolp, and P. van Genderen, "Improvement of target resolution in azimuth by lmmse technique," in *2009 European Radar Conference (EuRAD)*, Sept 2009, pp. 230–233.

[9] J. Guan, J. Yang, Y. Huang, and W. Li, "Maximum a posteriori based angular superresolution for scanning radar imaging," *IEEE Transactions on Aerospace and Electronic Systems*, vol. 50, no. 3, pp. 2389–2398, July 2014.

[10] D. L. Donoho, "Compressed sensing," *IEEE Transactions on Information Theory*, vol. 52, no. 4, April 2006.

[11] L. C. Potter, E. Ertin, J. T. Parker, and M. Cetin, "Sparsity and compressed sensing in radar imaging," *Proceedings of the IEEE*, vol. 98, no. 6, pp. 1006–1020, June 2010.

[12] M. A. Herman and T. Strohmer, "High-resolution radar via compressed sensing," *IEEE Transactions on Signal Processing*, vol. 57, no. 6, pp. 2275–2284, June 2009.

[13] X. Wen, G. Kuang, J. Hu, R. Zhan, and J. Zhang, "Forward-looking imaging of scanning phased array radar based on the compressed sensing," *Progress In Electromagnetics Research*, vol. 143, pp. 575–604, 2013.

[14] E. Candes and M. Wakin, "An introduction to compressive sampling," *Signal Processing Magazine, IEEE*, vol. 25, no. 2, pp. 21–30, 2008.

[15] R. Tibshirani, M. Saunders, S. Rosset, J. Zhu, and K. Knight, "Sparsity and smoothness via the fused LASSO," *Journal of the Royal Statistical Society Series B*, pp. 91–108, 2005.

[16] D. P. Bertsekas and J. N. Tsitsiklis. Parallel and Distributed Computation: Numerical Methods, 1997.

[17] M. Teichman, "Determination of horn antenna phase centers by edge diffraction theory," *IEEE Transactions on Aerospace and Electronic Systems*, vol. AES-9, no. 6, pp. 875–882, Nov 1973.